J Mater Sci (2017) 52:10738–10750

Chemical routes to materials

Pt–Se nanostructures with oxidase-like activity and their application in a selective colorimetric assay for mercury(II)

Leilei Guo[1], Long Mao[1], Kaixun Huang[1,2], and Hongmei Liu[1,2,*]

[1] Hubei Key Laboratory of Bioinorganic Chemistry and Materia Medica, School of Chemistry and Chemical Engineering, Huazhong University of Science and Technology, Wuhan 430074, People's Republic of China

[2] Key Laboratory of Material Chemistry for Energy Conversion and Storage, Ministry of Education, Wuhan 430074, People's Republic of China

Received: 7 January 2017
Accepted: 6 May 2017
Published online: 12 June 2017

ABSTRACT

In this paper, platinum (Pt)–selenium (Se) nanostructures and Pt nanoparticles were synthesized by a facile one-step chemical reduction route and their catalytic performance was evaluated as oxidase mimic. The results of structure characterization revealed that Pt–Se nanostructures consist of Pt and Se atoms (the Pt/Se atomic molar ratio is approximately 7:3), while Pt nanoparticles consist of pure element Pt. The oxidase-like activity of Pt–Se nanostructures and Pt nanoparticles was evaluated with 3,3′,5,5′-tetramethylbenzidine (TMB) as substrate. The results indicated that Pt–Se nanostructures had a lower Michaelis constant (K_m) and higher catalytic constant (K_{cat}) for TMB oxidation than that of Pt nanoparticles,which mean the binary Pt–Se hybrid nanostructures had stronger binding affinity with TMB and higher catalytic activity in comparison with monometallic Pt nanoparticles. The enhanced oxidase-like activity of Pt–Se nanostructures may be due to element Se doped in binary Pt–Se hybrid nanostructures, which can accelerate electron transport and provide excellent chemical stability against catalytic performance degradation during the TMB oxidation reaction. Mercury (II) ions (Hg^{2+}) could inhibit the oxidase mimetic activity of Pt–Se nanostructures and resulted in a color change of the reaction system. Based on this mechanism, a facile colorimetric assay for Hg^{2+} was developed with a detection limit as low as 70 nm and a linear range of 0–2.5 μM.

Introduction

Nanomaterials have attracted tremendous interest due to their unique physicochemical properties other than their bulk forms, including large surface-to-volume ratio, quantum size effect, surface plasmon resonance, and superparamagnetism. A number of work on the novel properties of nanomaterials impelled their extensive application in catalysis, photography, microelectronics, information storage,

Address correspondence to E-mail: hmliu2004@126.com

DOI 10.1007/s10853-017-1181-8

environmental protection, biological labeling, imaging, and sensing [1, 2]. In contrast, their potential as enzyme mimetic has long been ignored till ferromagnetic nanoparticles with intrinsic peroxidase-like activity were first reported in 2007 [3]. From then on, exploring and constructing nanomaterials mimic enzyme have attracted more and more attention due to their unique properties relative to nature enzyme. A variety of nanostructures, including FeSe, CuO, CeO_2, $CoFe_2O_4$, Co_3O_4 nanoparticles, graphene oxide, noble metal nanoparticles and their various hybrid nanostructures have been reported to have enzyme-like properties [4–9]. As compared to nature enzyme, nanomaterials artificial enzymes possess high stability against denaturing, excellent catalytic performance, together with easily synthesis and store in low cost. Thus, these mimic enzymes can replace nature enzyme using in many fields such as biosensor, colorimetric detection, immunoassays, cancer diagnostics, and pollutant degradation [10].

As an outstanding catalyst, Pt nanostructures have been found to possess various intrinsic enzyme-mimetic activity including peroxidase, oxidase, catalase, and superoxide dismutase [11, 12]. For instance, Cai et al. [13] adopted a facile method to synthesize porous Pt nanotube using tellurium nanowires as templates, and the porous Pt nanotube exhibits superior intrinsic peroxidase-like activity due to their specific surface area. Ultrafine lysozyme-stabilized Pt nanoclusters could catalyze the O_2 oxidation of typical organic substrates 3,3′,5,5′-tetramethylbenzidine (TMB) and dopamine as a mimic oxidase, which made their practical applicability in degrading methylene blue in the absence of H_2O_2 [14]. Pt nanoparticles also had catalase-like activity and significant superoxide dismutase-like activity of scavenging hydrogen peroxide and singlet oxygen under neutral conditions; these two enzymes play important roles in maintaining redox balance in living organisms by scavenging excess reactive oxygen species (ROS) [15].

In recent years, hybrid composite materials have been proved to exhibit enhanced mimic enzyme performance than their monometallic counterparts because of the synergistic effect, electronic structures effect, and the changes in the geometrical. Therefore, the development of Pt-based binary, ternary, and quaternary metallic systems including core–shell, alloy and cocatalysts to optimize the performance of Pt mimic enzyme has attracted considerable attention [16]. For example, a novel Au@Pt nanostructures synthesized as Au nanorods coated with a shell composed of Pt nanodots exhibited intrinsic oxidase-like, peroxidase-like, and catalase-like activity, which could be used in enzyme-linked immunosorbent assay (ELISA) for the detection of mouse interleukin 2 [17]. Wu reported that mercury (II) ions (Hg^{2+}) can inhibit the peroxidase-like activity of the DNA-Ag/Pt co-catalyst; therefore, DNA-Ag/Pt nanostructures could be used as a simple, rapid, and highly sensitive colorimetric assay for the detection of Hg^{2+} [18]. Au@PdPt nanostructures as PdPt alloy nanodots on gold nanorods possessed tuning oxidase-like activity via the composition of Pd/Pt ratio, which could catalyze the oxidation of TMB, Fe^{2+}, and ascorbic acid (AA) [19]. A novel aptamer stabilized Pt–Co bimetallic nanoparticle showed high oxidase-like catalytic activity, high water solubility, low cell toxicity, and superparamagnetic properties, which could be used as highly sensitive and selective colorimetric assay for cancer cell detection and other medical diagnosis [20].

Selenium (Se), an element of the chalcogenide group with novel chemical, physical, and biochemical properties, has been widely studied. Se is an essential trace element of fundamental importance to human health, such as the regulation of redox balance that is particularly important to cell growth and apoptosis [21]. Further, Se is also an excellent semiconductor with unique photoelectrical, photoconductivity, catalytic activity toward hydration, and oxidation, which promote its wide application in various fields such as xerography, semiconductor rectifiers, solar cells, and catalysis [22]. Due to its inspiring properties, element Se exhibits a lot of advantages as conventional heteroatom doping elements in a series catalyst. For instance, hybrid catalyst as element Se doped in noble metals (Au, Pt, Ag, and Ru) showed better stability and catalytic performance because of the anchor effect of Se [23–25]. Fuel cell catalysts modified with Se formed new catalytic active center due to the surface chemical interaction and charge transfer between Se and catalyst core [26, 27]. Furthermore, as Se atoms play a role in chemically stabilizing the Ru or Pt cluster core against oxidation, oxygen reduction reaction (ORR) catalyst (Ru- or Pt-based) with Se incorporation has high tolerance to methanol and overcome the catalyst poisoning [28, 29].

However, whether Pt–Se hybrid nanostructures have improved mimic enzyme performance remained unknown. In our previous work, we found for the first time that monometallic Se nanoparticles had intrinsic oxidase-like activity, which could catalyze the oxidization of TMB by dissolved oxygen [30]. Since both monometallic Pt nanoparticles and monometallic Se nanoparticles have oxidase-like activity, and a series catalyst modified with element Se showed increased stability and catalytic performance [25, 31, 32], it is reasonable to expect that Pt–Se hybrid nanostructures may possess enhanced oxidase-like activity due to synergistic effect of the bifunctional properties of the noble metal and the heteroatom. In order to confirm this speculation, Pt–Se nanostructures and Pt nanoparticles were synthesized and their oxidase-like activity was evaluated with TMB as a substrate in this work. The results indicated that Pt–Se nanostructures possess enhanced oxidase-like activity as compared to monometallic Pt nanoparticles. Furthermore, it was found that the oxidase mimic enzymatic activity of Pt–Se nanostructures could be inhibited by Hg^{2+}. Based on this phenomenon, a facile and rapid colorimetric detection for the sensing of Hg^{2+} was developed with a detection limit of 70 nm and a good linear range of 0–2.5 μM. The proposed method has highly sensitivity and selectivity toward Hg^{2+} over other common metal ions, which may have a potential application in detecting Hg^{2+} in environmental and biological samples.

Materials and methods

Materials

All chemicals were of analytical grade and used without further purification. Hexachloroplatinic acid ($H_2PtCl_6{\cdot}6H_2O$), polyvinylpyrrolidone (PVP), ascorbic acid, Na_2SeO_3, $NaBH_4$, $NaNO_3$, KNO_3, $Mn(CH_3COOH)_2{\cdot}7H_2O$, $Zn(NO_3)_2{\cdot}6H_2O$, $Cd(NO_3)_2{\cdot}4H_2O$, $CuSO_4$, $Pb(NO_3)_2$, $FeSO_4$, $FeCl_3{\cdot}6H_2O$, and $AlCl_3$ were purchased from Sinopharm Chemical Reagent Co., Ltd (Shanghai, China). $MgSO_4$ and $CaCl_2$ were purchased from Shanghai shiyi Chemical Reagent Co., Ltd. $Hg(NO_3)_2$ was purchased from General Research Institute for Nonferrous Metals. TMB was purchased from Aladdin (Shanghai, China). Doubled distilled water was used throughout the whole experiment.

Preparation of the Pt nanoparticles and Pt–Se nanostructures

In a typical synthesis of Pt nanoparticles, 1 mL of 5 mM H_2PtCl_6 was mixed with 1 mL of 50 mM PVP under vigorous stirring at room temperature, and then 1 mL of 50 mM $NaBH_4$ was added into the mixture. The reaction system was reconstituted to a final volume of 10 mL with doubled distilled water. The color of the mixture turned into dark brown, indicating the formation of Pt nanoparticles. In a typical synthesis of Pt–Se nanostructures, 17.6 mg of ascorbic acid was dissolved in 7 ml doubled distilled water; then 1 mL 5 mM H_2PtCl_6, 1 mL of 5 mM Na_2SeO_3, and 1 mL of 50 mM PVP were added to this solution. The mixed solution was under vigorous stirring for 2 h at room temperature until the color of the colloid became dark brown, which indicated the formation of Pt–Se nanostructures. The final concentration of Pt nanoparticles or Pt–Se nanostructures in the colloidal solution was 0.5 mM. Pt nanoparticles and Pt–Se nanostructures colloidal solution were washed with ethanol and acetone and then centrifuged at 10000 rpm for the removal of excess PVP. The precipitate was collected and resuspended in doubled distilled water to prepare Pt nanoparticles and Pt–Se nanostructures stock solution (3 mM).

Characterization of Pt nanoparticles and Pt–Se nanostructures

The as-obtained Pt nanoparticles and Pt–Se nanostructures were characterized by transmission electron microscopy (TEM), X-ray powder diffraction (XRD), dynamic light scattering (DLS), X-ray photoelectron spectroscopy (XPS), UV–Vis absorption, and fluorescence spectra. TEM sample was prepared by placing a drop of the colloidal dispersion onto a copper grid coated with a perforated carbon film, followed by evaporating the solvent at room temperature. Then the TEM graphs were obtained on a Tecnai (G2 20, FEI Co., Netherlands) at an acceleration voltage of 200 kV. The average particle size and the distribution were determined from about 200 particles of the enlarged micrographs. The mean hydrodynamic diameter of Pt nanoparticles and Pt–Se nanostructures in aqueous solution was obtained using a DLS instrument (LB-550, Horiba, Ltd. Japan). XRD patterns were recorded on an X-ray diffractometer (X'Pert PRO, PANalytical B.V., Netherlands) using

Cu Ka radiation with 40 kV and 55 mA in the 2θ range 10°–90°. The XPS sample was prepared by spreading the colloidal ethanol dispersion on a glass plate and dried under room temperature, and the XPS patterns were operated on an Axis-ultra Dld-600 W (Kratos, Japan) photoelectron spectrometer. UV–Vis absorption spectra were collected on a UV–Vis spectrophotometer (Shimadzu UV-2550) in the wavelength range of 200–600 nm. Fluorescence excitation and emission spectra were obtained on a JASCO FP-6200 fluorimeter.

Oxidase-like activity of Pt nanoparticles and Pt–Se nanostructures and kinetic studies

To investigate the oxidase-like activity of the as-synthesized Pt nanoparticles and Pt–Se nanostructures, the catalytic oxidation of the peroxidase substrate TMB in the absence of H_2O_2 was tested. In a typical experiment, 10 μL 3 mM Pt nanoparticles (5.8 μg Pt nanoparticles) or 10 μL 3 mM Pt–Se nanostructures (5.6 μg Pt–Se nanostructures) was mixed with 1.98 mL 0.2 M NaAc buffer; then 10 μL 4 g/L TMB was added to the mixture solution. As the reaction proceeded during 10 min, the blue color product of oxTMB was monitored in time scan mode at 652 nm using a Shimadzu UV-2450 spectrophotometer at an interval of 1 min [3]. The apparent kinetic parameters were calculated based on the Michaelis–Menten equation $V = V_{max} \times [S]/(K_m + [S])$, where V is the initial velocity, V_{max} is the maximal reaction velocity, $[S]$ is the concentration of substrate and K_m is the Michaelis constant. Catalytic constant (K_{cat}) as defined $K_{cat} = V_{max}/[E]_{total}$ was calculated, where $[E]_{total}$ is the molar concentration of Pt nanoparticles or Pt–Se nanostructures. To explore the optimal conditions of the oxidation of TMB with Pt nanoparticles and Pt–Se nanostructures, a range of temperatures (20–60 °C) and a range of pH values (2.7–5.6) for the reaction were measured under the same conditions mentioned above.

The application of Pt–Se nanostructures in colorimetric detection of Hg^{2+}

The detection of Hg^{2+} was carried out as follows. Ten microliter of 3 mM Pt–Se nanostructures and a series concentrations of Hg^{2+} were added into 2 mL 0.2 M NaAc buffer solution (pH 4.4). After 10 min of incubation, 15 μL of 4 g/L TMB was injected into the mixtures, and then the reaction system was incubated for another 10 min at 40 °C. The absorbance at 652 nm was recorded by a Shimadzu UV-2450 spectrophotometer.

To investigate the detection selectivity and sensibility of the method, effects of other metal ions, including Na^+, K^+, Mg^{2+}, Mn^{2+}, Zn^{2+}, Cd^{2+}, Ca^{2+}, Cu^{2+}, Pb^{2+}, Fe^{2+}, Fe^{3+}, and Al^{3+}, on the oxidase mimic activity of the Pt–Se nanostructures were also evaluated. In a typical experiment, 10 μL of 3 mM Pt–Se nanostructures and 10 μL of 10 mM different metal ions were added into 2 mL 0.2 M NaAc buffer solution (pH 4.4). After 10 min of incubation, 15 μL of 4 g/L TMB was injected into the mixtures and the reaction systems were incubated for another 10 min at 40 °C. The absorbance at 652 nm was recorded by a Shimadzu UV-2450 spectrophotometer.

Results and discussion

Characterization of Pt–Se nanostructures

Figure 1a, b shows the typical TEM image and DLS result of Pt nanoparticles, indicating that Pt nanoparticles possessed spherical-like morphology with narrow size distribution and an average size about 5.4 nm. As shown in Fig. 1c, d, the TEM image and DLS result revealed that Pt–Se nanostructures had irregular morphology with narrow size distribution and an average size about 13.5 nm. EDX attached to the TEM equipment was adopted to confirm the existence and the ratio of Pt/Se in Pt–Se nanostructures. As demonstrated in Fig. 1e, the quantitative analysis of EDX confirmed that Pt–Se nanostructures were consist of Pt and Se atoms, and the Pt/Se atomic molar ratio was approximately 7:3. Overall, the above results indicated that Pt nanoparticles and Pt–Se nanostructures displayed similar morphology only with differences on the size and composition.

Figure 2a shows XRD patterns of Pt nanoparticles and Pt–Se nanostructures. In the Pt nanoparticles spectrum, three diffraction peaks corresponding to the (111), (200), and (220) lattice planes were observed, which was consistent with the literature values (JCPDS 80-1268) [33]. In the Pt–Se nanostructures spectrum, the (111), (200), and (220) lattice planes could be also indexed, but with a small right

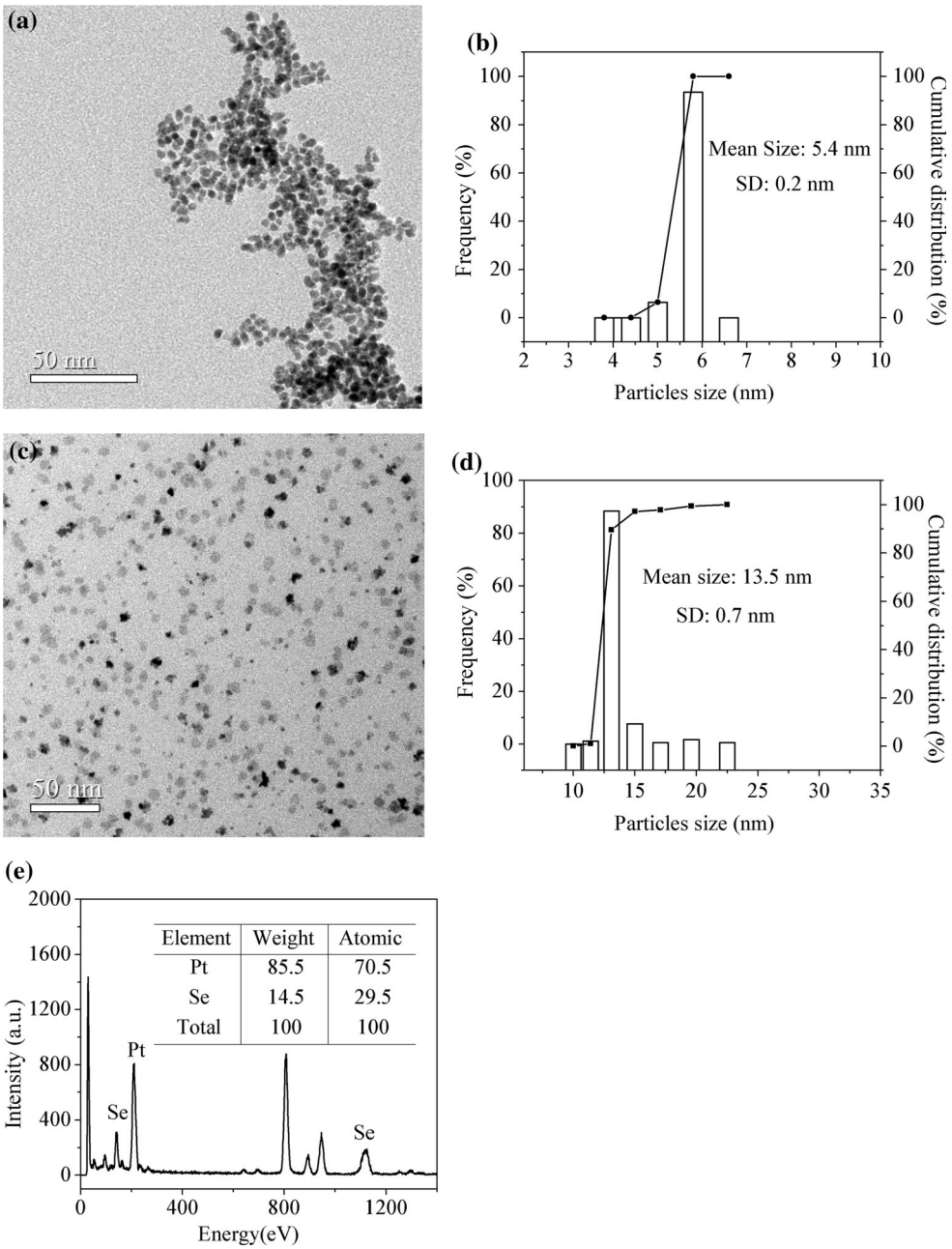

Figure 1 **a**, **b** TEM image (the *scale bar* was 50 nm) and DLS result of Pt nanoparticles; **c**, **d** TEM images (the *scale bar* was 50 nm) and DLS result of Pt–Se nanostructures; **e** EDX of Pt–Se nanostructures.

shift, which may be due to the doped Se. This result indicated that Pt–Se nanostructures formed with doped Se might possess similar crystal form with pure Pt nanoparticles. It was worth noting that element Se might exist as amorphous form in the Pt–Se nanostructures, but its typical diffraction peak was not present in the XRD pattern [30].

To further investigate the composition of Pt–Se nanostructures, XPS spectrum of the Pt 4f region and Se 3d region was collected. The typical Pt $4f_{7/2}$ and Pt $4f_{5/2}$ binding energy was about 70.8 eV and 74.2 eV in Pt nanoparticles (Fig. 2b), which is indicative of the reduced platinum Pt (0). The XPS spectrum of Pt 4f region in Pt–Se nanostructures (Fig. 2c) revealed the similar result, with Pt $4f_{7/2}$ peak at about 71.5 eV and Pt $4f_{5/2}$ peak at 74.4 eV, respectively. This result showed that Pt–Se nanostructures were composed of element Pt (0). The XPS spectrum of Se 3d region in Pt–Se nanostructures showed that the 3d orbit binding energy of Se was about 55.1 eV (Fig. 2d), which was consistent with the standard value of element Se (0). Therefore, it could be clearly observed that Pt–Se

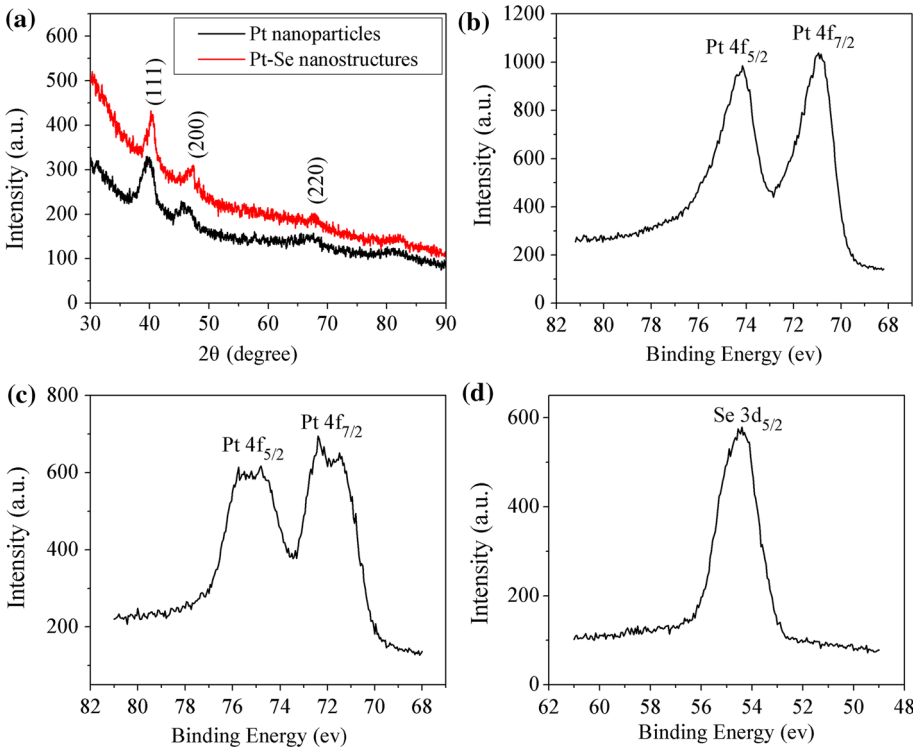

Figure 2 **a** XRD patterns of Pt nanoparticles and Pt–Se nanostructures; **b** XPS spectrum of Pt 4f region in Pt nanoparticles; **c** XPS spectrum of Pt 4f region in Pt–Se nanostructures; **d** XPS spectrum of Se 3d region in Pt–Se nanostructures.

nanostructures were consist of reduced platinum Pt (0)- and Se (0)-based on the XPS results.

Figure 3a shows the UV–Vis spectra change during the formation of Pt nanoparticles and Pt–Se nanostructures. The H_2PtCl_6 aqueous solution was pale yellow and shows a peak at about 265 nm in its UV–Vis spectrum (green line in Fig. 3a) due to the ligand-to-metal charge transfer transition of the $[PtCl_6]^{2-}$ ions [14]. After the addition of reduction agent $NaBH_4$, the color of the solution turned into dark brown within 30 min. The UV–Vis spectrum showed the peak at 265 nm disappeared (blue line in Fig. 3a), indicating that the $[PtCl_6]^{2-}$ ions were completely reduced and the Pt nanoparticles was formed. On the other hand, the mixture solution of H_2PtCl_6 and Na_2SeO_3 showed nearly the same absorption spectrum with H_2PtCl_6 aqueous solution (black line in Fig. 3a), indicating that there was no interaction with H_2PtCl_6 and Na_2SeO_3 before reaction. After the addition of reduction agent ascorbic acid, the peak at 265 nm was also disappeared and the absorption from the visible region to the ultraviolet increased along with the formation of dark brown solution (red line in Fig. 3a). It was worth noting that there appeared an absorption peak at nearly 300 nm, which was relevant to the formation vibration of Se nanoparticles [34]. Based on the UV–Vis spectrum of Pt–Se nanostructures, it could be seen that Pt nanoparticles and Se nanoparticles coexist during the process of Pt–Se nanostructure formation. In order to

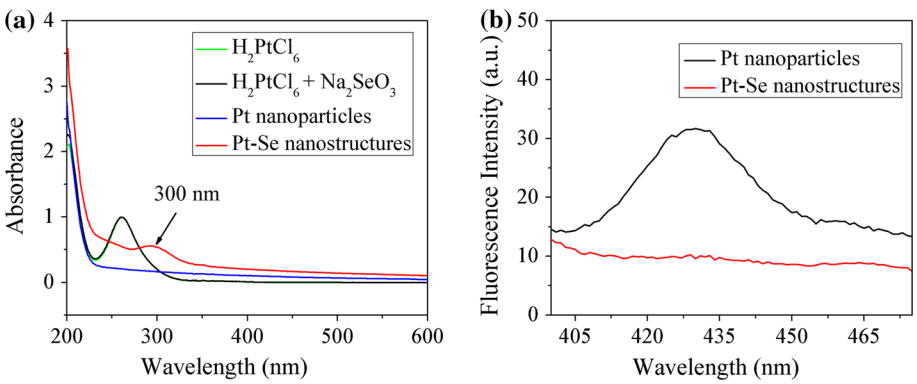

Figure 3 **a** UV–Vis spectra change during the formation of Pt nanoparticles and Pt–Se nanostructures; **b** fluorescence spectra obtained from the synthesis of Pt nanoparticles and Pt–Se nanostructures.

further investigate the structure effect of element Se nanoparticles doped in the Pt–Se nanostructures, fluorescence spectra of Pt nanoparticles and Pt–Se nanostructures are shown in Fig. 3b. The maximal emission wavelength of Pt nanoparticles was about 435 nm as the excitation wavelength fixed in 350 nm, while the maximal emission wavelength at 435 nm disappeared for the Pt–Se nanostructures. The fluorescence quenching for Pt–Se nanostructures may be due to doped Se in the Pt nanoparticles.

The enhanced oxidase-like activity of Pt–Se nanostructures

The oxidase-like activity of Pt nanoparticles and Pt–Se nanostructures was evaluated in the catalysis of typical substrate TMB in the absence of H_2O_2. As shown in Fig. 4a, Pt nanoparticles and Pt–Se nanostructures could catalyze the oxidation of TMB with dissolved O_2 in NaAc buffer to produce a typical blue color product during 10 min, suggesting the oxidase-like activity of the as-synthesized Pt nanoparticles and Pt–Se nanostructures. In addition, the Pt–Se nanostructures showed significantly higher oxidase-like activity than Pt nanoparticles, since much more blue product was obtained in the Pt–Se nanostructures system than that in Pt nanoparticles system under the same reaction conditions. Pt–Se nanostructures with enhanced oxidase-like activity could also be confirmed by UV–Vis spectra. As can be seen from Fig. 4b, the maximum absorbance peak of the blue color products of TMB oxidation was located at 652 nm; the absorbance of the Pt–Se nanostructures system was much higher, indicating that the activity of Pt–Se nanostructures was significantly enhanced in comparison with Pt nanoparticles. The initial oxidation rates of Pt nanoparticles and Pt–Se nanostructures were evaluated by monitoring the time course of absorbance at 625 nm (Fig. 4c). The absorbance of the oxidized TMB at 652 nm was continuously increased in the presence of Pt nanoparticles or Pt–Se nanostructures as the reaction time extended, while the absorbance of the reaction system without catalyst nearly unchanged. As evaluated from the absorbance of oxidized TMB, the catalytic activity of the Pt–Se nanostructures was nearly two times that of Pt nanoparticles.

Similar to other oxidase and peroxidase mimics, the catalytic activities of Pt nanoparticles and Pt–Se nanostructures were also dependent on pH and temperature. Figure 5a shows the effect of pH on the oxidase-like activity of Pt nanoparticles and Pt–Se

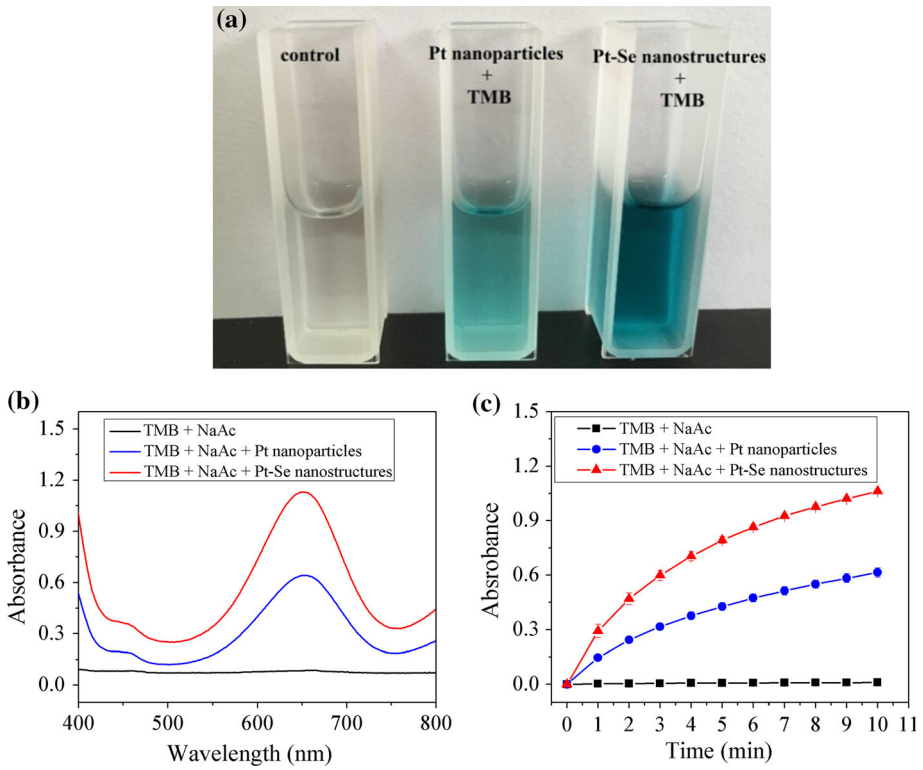

Figure 4 **a** Color evolutions of TMB oxidation catalyzed by Pt nanoparticles and Pt–Se nanostructures. **b** The UV–visible absorption spectra of TMB-derived oxidation product in the presence of Pt nanoparticles or Pt–Se nanostructures. **c** Time-dependent absorbance changes at 652 nm in the presence of Pt nanoparticles or Pt–Se nanostructures (black curve in **b**, **c** represents the control experiment without catalyst). Conditions: [TMB] = 83.2 μM, [Pt] or [PtSe] = 15 μM.

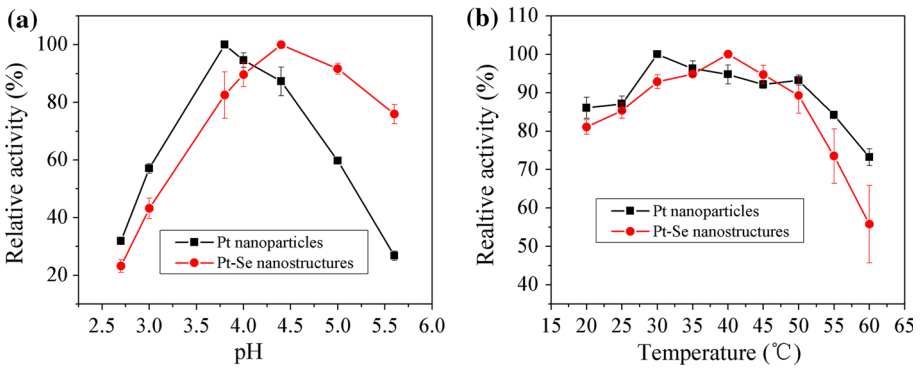

Figure 5 **a** Effect of pH on the oxidase-like activity of Pt nanoparticles and Pt–Se nanostructures. Conditions: [TMB] = 83.2 μM, [Pt] or [PtSe] = 15 μM. **b** Effect of temperature on the oxidase-like activity of Pt nanoparticles and Pt–Se nanostructures. Conditions: [TMB] = 83.2 μM, [Pt] or [PtSe] = 15 μM.

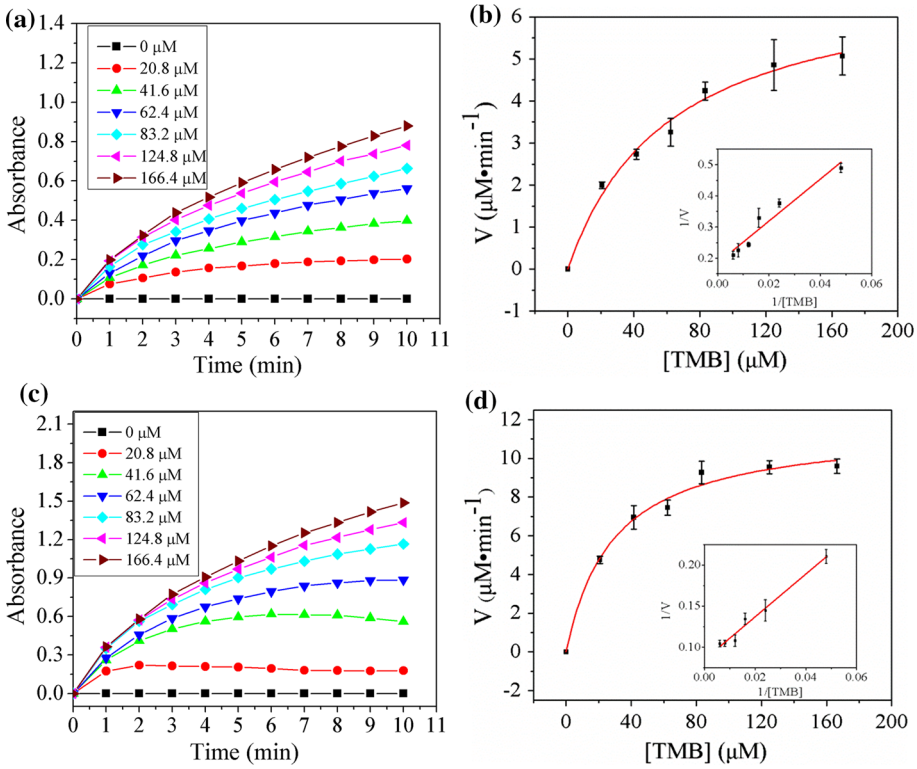

Figure 6 **a** Time-dependent absorbance changes at 652 nm of various concentrations of TMB for Pt nanoparticles. **b** The steady-state kinetic assay of Pt nanoparticles with TMB. **c** Time-dependent absorbance changes at 652 nm of various concentrations of TMB for Pt–Se nanostructures. **d** The steady-state kinetic assay for Pt–Se nanostructures with TMB. *Inset* for **b**, **d** double reciprocal plots between reaction velocity and TMB concentration. Conditions: [Pt] or [PtSe] = 15 μM.

nanostructures in a pH range from 2.7 to 5.6. The results showed that the maximum catalytic activity for Pt nanoparticles and Pt–Se nanostructures was at pH 3.8 and 4.4, respectively. And, more remarkable, Pt–Se nanostructures exhibited more steady catalytic activity than Pt nanoparticles at a pH range of 3.8–5.6. The oxidase-like activity of Pt–Se nanostructures remained about 78% at pH 5.6 compared to that of optimum pH 4.4. As a contrast, the Pt nanoparticles lost almost 80% of its activity at pH 5.6 compared to that of optimum pH 3.8. Different pH can affect the formation of different hydration shell water in the surface of nanomaterials, which may result in the pH-dependent activity of nanoenzyme [35]. Furthermore, Pt nanoparticles and Pt–Se nanostructures with maximum catalytic activity at different pH were likely attributed to their different composition. The as-synthesized Pt–Se hybrid nanostructures may affect the interaction between nanomaterials mimic enzyme and substrate TMB, thereby achieving the

synergistic effect between Pt nanoparticles and Se nanoparticles.

Effects of temperature on the oxidase-like activity of Pt nanoparticles and Pt–Se nanostructures were examined in a temperature range from 20 to 60 °C. As seen in Fig. 5b, both Pt nanoparticles and Pt–Se nanostructures remained high oxidase-like activity in the range of 20–60 °C, and the optimum temperature for Pt nanoparticles and Pt–Se nanostructures was 30 and 40 °C, respectively. The catalytic activity of Pt nanoparticles and Pt–Se nanostructures then decreased as the temperature increased above 50 °C, and Pt–Se nanostructures lost more activity as compared to Pt nanoparticles. Temperature can not only alter the reaction efficiency, but also affect the stability and structure of the nanoparticles involved in the catalytic reaction. More catalytic sites of Pt nanoparticles and Pt–Se nanostructures were activated with increased temperature, leading to increase of catalytic activity. Furthermore, higher temperature can provide more energy for the bonding of catalyst and substrate. However, too high temperature may bring about the agglomeration of nanoparticles and cause the loss of stability, which resulted in the significant decrease of catalytic activity. Previous study showed that the structure of Se nanoparticles may transform into t-Se crystal with the increased size under excessive high temperature [36]. Therefore, due to the variation of crystal form and size of element Se under high temperature, the construction of Pt–Se nanostructure may be destroyed, resulting in the loss of synergistic effect between Pt nanoparticles and Se nanoparticles. It may be the reason that the Pt–Se nanostructures exhibited greater deterioration of catalytic activity in comparison with Pt nanoparticles when the temperature was above 50 °C.

To further comparing the catalytic activity and acquiring kinetic parameters of Pt nanoparticles and Pt–Se nanostructures, the apparent steady-state kinetic parameters of TMB were obtained by varying TMB concentration. As shown in Fig. 6, a typical Michaelis–Menten curve was obtained with TMB by recording the absorbance change at 652 nm for 10 min at an interval of 1 min. The Michaelis–Menten constant (K_m) and maximum initial velocity (V_{max}) were obtained using a Lineweaver–Burk plot. The K_m value of Pt–Se nanostructures with TMB as the substrate was lower than that of Pt nanoparticles (0.029 mM to 0.051 mM), and the catalytic constant(K_{cat}) of Pt–Se nanostructures was nearly 2 times of that of Pt nanoparticles (as shown in Table 1). K_m is an important parameter for measuring binding affinity of the enzyme to the substrates and affects the value of the reaction rate. A low K_m means the strong affinity of the enzyme to the substrates and vice versa. Therefore, our data demonstrated that Pt–Se nanostructures had higher affinity for TMB than that of Pt nanoparticles, which provided an explanation for the enhanced catalytic activity of Pt–Se nanostructures.

The element Se doped in binary Pt–Se hybrid nanostructures might play a vital role in their enhanced oxidase-like activity. Previous researches showed that Se had several advantages as conventional heteroatom doping elements. For instance, the excellent electric conductivity of Se can accelerate electron transport, and the anchoring effect of Se atom can enhance the stability of catalyst [27, 28]. Furthermore, Se can become metallic when bound to metals resulting in exceptional chemical stability in acidic media due to the charge transfer between metal and Se [26, 29]. Therefore, element Se doped in Pt–Se nanostructures might accelerate electron transport between the electron donor TMB and the electron acceptor oxygen. Additionally, the anchoring effect of heteroatom Se might enhance the tolerance of Pt for oxidation products. Anyway, the exact role of doped Se in the enhanced catalytic activity of Pt–Se nanostructures should be studied in depth in the future.

Table 1 Apparent kinetic parameters of Pt nanoparticles and Pt–Se nanostructures as oxidase mimics for TMB oxidation

	$[E]_{total}$ (μM)	K_m (mM)	V_{max} (μM min^{-1})	K_{cat} (min^{-1})
Pt nanoparticles	15	0.051	6.52	0.43
Pt–Se nanostructures	15	0.029	11.69	0.78

$[E]_{total}$ is the molar concentration of Pt nanoparticles or Pt–Se nanostructures. K_m is the Michaelis constant, and V_{max} is the maximal reaction velocity. K_{cat} is the catalytic constant, where $K_{cat} = V_{max}/[E]_{total}$

The application of Pt–Se nanostructures in a selective colorimetric assay for Hg^{2+}

As one of the most toxic heavy metal ions, Hg^{2+} can lead to great harm to human health and environment due to their intrinsic bioaccumulation property. Various detection methods including chemiluminescence, fluorescent, and electrochemical assays have been utilized to improve the detection sensitivity and selectivity of Hg^{2+} [37]. Recently, it was found that Hg^{2+} possesses strong interaction with active site/center of enzymes and causes the inhibition or stimulation of their catalytic activity. Therefore, colorimetric detections of Hg^{2+} on basis of nanomaterials mimic enzyme have become a novel and facile method [38, 39]. In our work, it was found that the oxidase mimetic activity of Pt–Se nanostructures could be inhibited by Hg^{2+}, as shown in Fig. 7a. The absorbance at 652 nm decreased sharply as the concentration of Hg^{2+} ranging from 0 to 10 μM. As Hg^{2+} concentrations were over 10 μM, the inhibition of Hg^{2+} to the catalytic activity of Pt–Se nanostructures leveled off. Notably, it could be observed a good linear relationship between the absorbance at 652 nm and Hg^{2+} concentrations in the range of 0–2.5 μM (the inset in Fig. 7a), with the linear calibration plot of $A_{652} = 1.0449–0.0002[Hg^{2+}]$ ($R^2 = 0.992$). The detection limit of Hg^{2+} using this method is 70 nM as the signal-to-noise ratio is 3, according to the equation: the detection limit $= 3\sigma/\text{slope}$ [38]. The slope obtained from the linear calibration plot, and the σ represented the blank standard deviation. The repeatability expressed as the relative standard deviation (RSD) was 0.92% ($n = 15$). This colorimetric assay for Hg^{2+} using Pt–Se nanostructures showed a lower detection limit and higher sensitivity in comparison with some other nanomaterial-based colorimetric assay [40–45].

To evaluate the selectivity of the colorimetric assay for Hg^{2+}, various common metal ions including Na^+, K^+, Mg^{2+}, Mn^{2+}, Zn^{2+}, Cd^{2+}, Ca^{2+}, Cu^{2+}, Pb^{2+}, Fe^{2+}, Fe^{3+}, and Al^{3+} were used to investigate their effect on the oxidase-like activity of Pt–Se nanostructures. As shown in Fig. 7b, even at 50 μM (in comparison with 5 μM Hg^{2+}), other metal ions showed no obvious inhibition or stimulation to the oxidase mimetic activity of the Pt–Se nanostructures. Therefore, the colorimetric assay using Pt–Se nanostructures mimic enzyme exhibited high selectivity toward Hg^{2+} over other metal ions. Based on these data, Pt–Se nanostructures can be utilized as a potential candidate for the detection of Hg^{2+} with high sensitivity and selectivity.

Previous studies showed that Hg^{2+} ions could alter the surface properties of Au, Ag, and Pt nanoparticles through the strongest Hg^{2+}-noble metal nanoparticles interaction, which led to the inhibition of their catalytic activity [37, 46]. In our colorimetric assay,

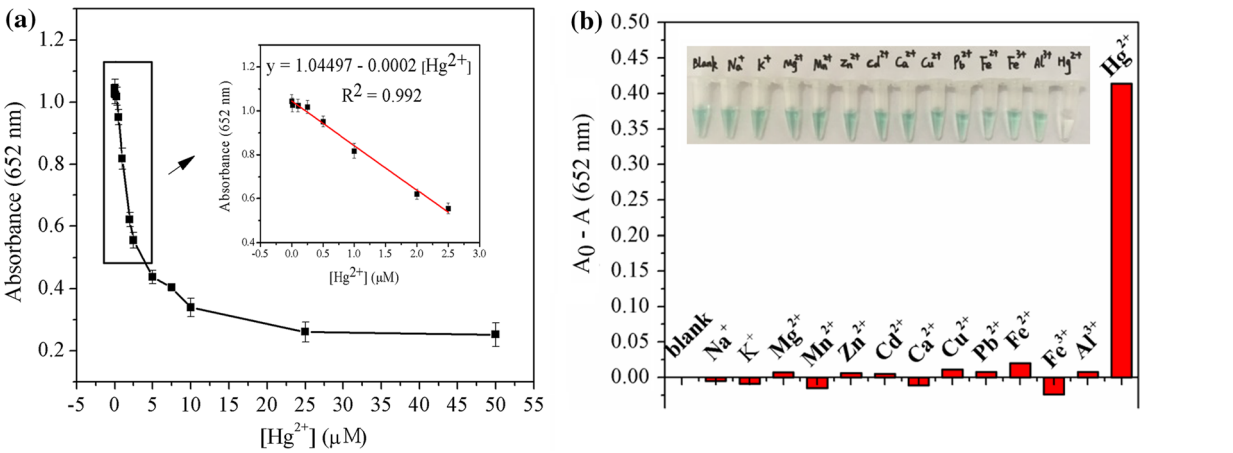

Figure 7 **a** Curve of the A_{652} values with Pt–Se nanostructures in the presence of different concentrations of Hg^{2+}, *inset*: linear calibration plot for Hg^{2+} detection. Conditions: [TMB] = 83.2 μM, [PtSe] = 15 μM, pH 4.4 NaAc, reaction temperature 40 °C. **b** Effects of metal ions on the oxidase-like activity of Pt–Se nanostructure. A represents the absorbance of oxTMB at 652 nm in the presence of Pt–Se nanostructure and different metal ions. A_0 represents the absorbance of oxTMB at 652 nm in the presence of Pt–Se nanostructure. [Hg^{2+}]: 5 μM; other metal ions: 50 μM. The reaction system was in pH 4.4 NaAc buffer solution including 15 μM Pt–Se nanostructure and 83.2 μM TMB. The *inset* shows the corresponding color evolutions of TMB oxidation catalyzed by Pt–Se nanostructure in the presence of various metal ions.

the notable inhibition of Hg^{2+} on oxidase-like activity of Pt–Se nanostructures may be attributed to the interaction of Hg^{2+} and Pt–Se nanostructures. Hg^{2+} may interact with Pt–Se nanostructures through its well-known metallophilic property and cause the formation of Hg/Pt amalgam. Thus, the content of Pt(0) in the Pt–Se nanostructures decreased in quantity, and a number of oxidase mimetic active centers of Pt–Se nanostructures may be blocked, which resulted in the inhibition of the Pt–Se mimic enzyme catalytic activity. Furthermore, we observed obvious agglomeration of Pt–Se nanostructures after addition of 50 μM Hg^{2+}. This means that Hg^{2+} destroyed the surface electrical structure of Pt–Se nanostructures, leading to the decrease of the stability of the Pt–Se nanostructures.

Conclusion

In conclusion, Pt–Se nanostructures and Pt nanoparticles were synthesized by a one-step chemical reduction route in aqueous solution using PVP as protective agent. The Pt–Se nanostructures with a mean diameter of about 13.5 nm formed as the Pt/Se atomic molar ratio are approximately 7:3, while the Pt nanoparticles consist of pure element Pt with a mean diameter of about 5.4 nm. The oxidase-like activity of Pt–Se nanostructures and Pt nanoparticles was evaluated with TMB as substrate. The data exhibited that Pt–Se nanostructures had an optimum catalytic activity at pH 4.4 and 40 °C, while Pt nanoparticles were at pH 3.8 and 30 °C. The maximum catalytic activity at different pH and temperature for the two nanomaterials was likely attributed to different composition and size. The K_m values and K_{cat} of Pt–Se nanostructures for TMB oxidation were 0.029 mM and 0.78 min^{-1}, while the K_m values and K_{cat} of Pt nanoparticles for TMB were 0.051 mM and 0.43 min^{-1}. The lower K_m value and higher K_{cat} mean Pt–Se nanostructures have stronger binding affinity with the substrate TMB and higher catalytic activity in comparison with Pt nanoparticles. The enhanced oxidase-like activity of Pt–Se nanostructures may be attributed to element Se doped for the formation of binary Pt–Se hybrid nanostructures. The binary Pt–Se hybrid nanostructures can provide more active sites for the substrate adsorption and accelerate electron transport; the anchor effect of element Se provides the exceptional chemical stability. In a word, Pt–Se nanostructures with enhanced oxidase-like activity can be achieved due to synergistic effect of the noble metal and the heteroatom. As compared to other Pt-based (Au, Pd and Ag) hybrid nanostructures mimic enzyme, Pt–Se nanostructures can achieve the similar oxidase-like activity. Furthermore, the oxidase mimic enzymatic activity of Pt–Se nanostructures could be efficiently inhibited by Hg^{2+} through the metallophilic interactions, which bring about a facile and rapid colorimetric detection for Hg^{2+} with a detection limit of 70 nm and a good linear range of 0–2.5 μM. The proposed method has high sensitivity and selectivity toward Hg^{2+} over other common metal ions, which promotes Pt–Se nanostructures that can be utilized as a potential candidate for detecting Hg^{2+} in environmental and biological samples.

Acknowledgements

We thank the faculties from Analytical and Testing Center of Huazhong University of Science and Technology for help in the operation of TEM, EDX, XRD, and XPS. We also thank the faculties from Analytical and Testing Center of School of Chemistry and Chemical Engineering for help in the operation of DLS, UV–Vis spectrophotometer, and fluorescence spectrophotometer. This work was supported by the "Youth Chen-Guang Project" of Wuhan Bureau of Science and Technology (Grant No. 2015070404010184) and Natural Science Foundation of Hubei Scientific Committee (Grant No. 2016CFA001).

References

[1] Asefa T, Duncan CT, Sharma KK (2009) Recent advances in nanostructured chemosensors and biosensors. The Analyst 134:1980–1990

[2] Xia Y, Xiong Y, Lim B, Skrabalak SE (2009) Shape-controlled synthesis of metal nanocrystals: simple chemistry meets complex physics? Angew Chem Int Ed 48:60–103

[3] Gao L, Zhuang J, Nie L, Zhang J, Zhang Y, Gu N, Wang T, Feng J, Yang D, Perrett S, Yan X (2007) Intrinsic peroxidase-like activity of ferromagnetic nanoparticles. Nat Nanotechnol 2:577–583

[4] Dutta AK, Maji SK, Srivastava DN, Mondal A, Biswas P, Paul P, Adhikary B (2012) Synthesis of FeS and FeSe nanoparticles from a single source precursor: a study of their

photocatalytic activity, peroxidase-like behavior, and electrochemical sensing of H_2O_2. ACS Appl Mater Interf 4:1919–1927

[5] Feng YB, Hong L, Liu AL, Chen WD, Li GW, Chen W, Xia XH (2015) High-efficiency catalytic degradation of phenol based on the peroxidase-like activity of cupric oxide nanoparticles. Int J Environ Sci Technol 12:653–660

[6] Hayat A, Cunningham J, Bulbul G, Andreescu S (2015) Evaluation of the oxidase like activity of nanoceria and its application in colorimetric assays. Anal Chim Acta 885:140–147

[7] Lin Y, Ren J, Qu X (2014) Catalytically active nanomaterials: a promising candidate for artificial enzymes. Acc Chem Res 47:1097–1105

[8] Zhang X, He S, Chen Z, Huang Y (2013) $CoFe_2O_4$ nanoparticles as oxidase mimic-mediated chemiluminescence of aqueous luminol for sulfite in white wines. J Agric Food Chem 61:840–847

[9] Lin Y, Ren J, Qu X (2014) Catalytically active nanomaterials: a promising candidate for artificial enzymes. Acc Chem Res 47:1097–1105

[10] Xie J, Zhang X, Wang H, Zheng H, Huang Y, Xie J (2012) Analytical and environmental applications of nanoparticles as enzyme mimetics. Trends Anal Chem 39:114–129

[11] Liu Y, Wu H, Chong Y, Wamer WG, Xia Q, Cai L, Nie Z, Fu PP, Yin JJ (2015) Platinum nanoparticles: efficient and stable catechol oxidase mimetics. ACS Appl Mater Interf 7:19709–19717

[12] Liu Y, Wu H, Li M, Yin JJ, Nie Z (2014) pH dependent catalytic activities of platinum nanoparticles with respect to the decomposition of hydrogen peroxide and scavenging of superoxide and singlet oxygen. Nanoscale 6:11904–11910

[13] Cai K, Lv Z, Chen K, Huang L, Wang J, Shao F, Wang Y, Han H (2013) Aqueous synthesis of porous platinum nanotubes at room temperature and their intrinsic peroxidase-like activity. Chem Commun 49:6024–6026

[14] Yu CJ, Chen TH, Jiang JY, Tseng WL (2014) Lysozyme-directed synthesis of platinum nanoclusters as a mimic oxidase. Nanoscale 6:9618–9624

[15] Fan J, Yin JJ, Ning B, Wu X, Hu Y, Ferrari M, Anderson GJ, Wei J, Zhao Y, Nie G (2011) Direct evidence for catalase and peroxidase activities of ferritin–platinum nanoparticles. Biomaterials 32:1611–1618

[16] Peng Z, Yang H (2009) Designer platinum nanoparticles: control of shape, composition in alloy, nanostructure and electrocatalytic property. Nano Today 4:143–164

[17] He W, Liu Y, Yuan J, Yin JJ, Wu X, Hu X, Zhang K, Liu J, Chen C, Ji Y, Guo Y (2011) Au@Pt nanostructures as oxidase and peroxidase mimetics for use in immunoassays. Biomaterials 32:1139–1147

[18] Wu L-L, Wang L-Y, Xie Z-J, Xue F, Peng C-F (2016) Colorimetric detection of Hg^{2+} based on inhibiting the peroxidase-like activity of DNA–Ag/Pt nanoclusters. RSC Adv 6:75384–75389

[19] Zhang K, Hu X, Liu J, Yin JJ, Hou S, Wen T, He W, Ji Y, Guo Y, Wang Q, Wu X (2011) Formation of PdPt alloy nanodots on gold nanorods: tuning oxidase-like activities via composition. Langmuir ACS J Surf Colloids 27:2796–2803

[20] Cai S, Qi C, Li Y, Han Q, Yang R, Wang C (2016) PtCo bimetallic nanoparticles with high oxidase-like catalytic activity and their applications for magnetic-enhanced colorimetric biosensing. J Mater Chem B 4:1869–1877

[21] Rayman MP (2012) Selenium and human health. The Lancet 379:1256–1268

[22] Ray C, Dutta S, Sarkar S, Sahoo R, Roy A, Pal T (2013) A facile synthesis of 1D nano structured selenium and Au decorated nano selenium: catalysts for the clock reaction. RSC Adv 3:24313–24320

[23] Shih Z-Y, Yang Z, Lin Z-H, Chang H-T (2011) Direct methanol fuel cells using Se/Ru core/shell cathodes provide high catalytic activity and stability. Int J Hydrogen Energy 36:7303–7309

[24] Yang L, Shen Y, Xie A, Liang J, Zhu J, Chen L (2007) Synthesis of controllable-size core–shell Se@Ag and Se@Au nanoparticles in UV-Irradiated TSA solution. Eur J Inorg Chem 2007:1128–1134

[25] Ma J, Canaff C, Alonso-Vante N (2014) The effect of tuning and origin of tolerance to organics of platinum catalytic centers modified by selenium. Phys Status Solidi A 211:2030–2034

[26] Babu PK, Lewera A, Chung JH, Hunger R, Jaegermann W (2007) Selenium becomes metallic in Ru–Se fuel cell catalysts: an EC-NMR and XPS investigation. J Am Chem Soc 129:15140–15141

[27] Inukai J, Cao D, Wieckowski A, Chang K-C, Menzel A, Komanicky V, You H (2007) In situ synchrotron X-ray spectroscopy of ruthenium nanoparticles modified with selenium for an oxygen reduction reaction. J Phys Chem C 111:16889–16894

[28] Wang R, Da H, Wang H, Ji S, Tian Z (2013) Selenium functionalized carbon for high dispersion of platinum–ruthenium nanoparticles and its effect on the electrocatalytic oxidation of methanol. J Power Sources 233:326–330

[29] Wang H, Da H, Ji S, Liao S, Wang R (2013) Selenium-functionalized carbon as a support for platinum nanoparticles with improved electrochemical properties for the oxygen reduction reaction and CO tolerance. J Electrochem Soc 160:266–270

[30] Guo L, Huang K, Liu H (2016) Biocompatibility selenium nanoparticles with an intrinsic oxidase-like activity. J Nanopart Res 18:1–10. doi:10.1007/s11051-016-3357-6

[31] Ahluwalia S, Prakash NT, Prakash R, Pal B (2016) Improved degradation of methyl orange dye using bio-co-catalyst Se nanoparticles impregnated ZnS photocatalyst under UV irradiation. Chem Eng J 306:1041–1048

[32] Chang T-W, Wang C-W, Chen C-H, Li Y-C, Hsu C-L, Chang H-T, Lin Z-H (2016) Controlled synthesis of Se-supported Au/Pd nanoparticles with photo-assisted electrocatalytic activity and their application in self-powered sensing systems. Nano Energy 22:564–571

[33] Peng Z, Wu J, Yang H (2010) Synthesis and oxygen reduction electrocatalytic property of platinum hollow and platinum-on-silver nanoparticles. Chem Mater 22:1099–1106

[34] Tran PA, O'Brien-Simpson N, Reynolds EC, Pantarat N, Biswas DP, O'Connor AJ (2016) Low cytotoxic trace element selenium nanoparticles and their differential antimicrobial properties against *S. aureus* and *E. coli*. Nanotechnology 27:1–10

[35] Yang M, Guan Y, Yang Y, Xia T, Xiong W, Wang N, Guo C (2013) Peroxidase-like activity of amino-functionalized magnetic nanoparticles and their applications in immunoassay. J Colloid Interface Sci 405:291–295

[36] Chen H, Yoo J-B, Liu Y, Zhao G (2012) Green synthesis and characterization of se nanoparticles and nanorods. Electron Mater Lett 7:333–336

[37] Sun Z, Zhang N, Si Y, Li S, Wen J, Zhu X, Wang H (2014) High-throughput colorimetric assays for mercury(II) in blood and wastewater based on the mercury-stimulated catalytic activity of small silver nanoparticles in a temperature-switchable gelatin matrix. Chem Commun 50:9196–9199

[38] Li W, Chen B, Zhang H, Sun Y, Wang J, Zhang J, Fu Y (2015) BSA-stabilized Pt nanozyme for peroxidase mimetics and its application on colorimetric detection of mercury(II) ions. Biosens Bioelectron 66:251–258

[39] Yan L, Chen Z, Zhang Z, Qu C, Chen L, Shen D (2013) Fluorescent sensing of mercury(II) based on formation of catalytic gold nanoparticles. The Analyst 138:4280–4283

[40] Chen X, Zhai N, Snyder JH, Chen Q, Liu P, Jin L, Zheng Q, Lin F, Hu J, Zhou H (2015) Colorimetric detection of Hg^{2+} and Pb^{2+} based on peroxidase-like activity of graphene oxide–gold nanohybrids. Anal Methods 7:1951–1957

[41] Farhadi K, Forough M, Molaei R, Hajizadeh S, Rafipour A (2012) Highly selective Hg^{2+} colorimetric sensor using green synthesized and unmodified silver nanoparticles. Sensors Actuators B: Chem 161:880–885

[42] Jayabal S, Sathiyamurthi R, Ramaraj R (2014) Selective sensing of Hg^{2+} ions by optical and colorimetric methods using gold nanorods embedded in a functionalized silicate sol–gel matrix. J Mater Chem A 2:8918–8925

[43] Wang Y, Yang F, Yang X (2010) Colorimetric biosensing of mercury(II) ion using unmodified gold nanoparticle probes and thrombin-binding aptamer. Biosens Bioelectron 25:1994–1998

[44] Yang H, Xiong Y, Zhang P, Su L, Ye F (2015) Colorimetric detection of mercury ions using MnO_2 nanorods as enzyme mimics. Anal Methods 7:4596–4601

[45] Lee JS, Han MS, Mirkin CA (2007) Colorimetric detection of mercuric ion (Hg^{2+}) in aqueous media using DNA-functionalized gold nanoparticles. Angew Chem 46:4093–4096

[46] Long YJ, Li YF, Liu Y, Zheng JJ, Tang J, Huang CZ (2011) Visual observation of the mercury-stimulated peroxidase mimetic activity of gold nanoparticles. Chem Commun 47:11939–11941